We thank the reviewers for their comments. Below are our responses in blue.

Reviewer 1

The paper investigates the value of DAR for retrieving integrated water vapour (IWV). The paper is concise, well written and generally clear. The topic is very important and timely given the recent technology advance for G-band radars. I have few major points that I would like to be addressed.

Major comments:

1) The paper provides a good idea about the performance of the proposed DAR system globally. However the strength/novelty of the methodology to me is to provide IWV in cloudy conditions (in clear sky conditions we can probably be satisfied with current observations), where also I expect to see larger IWV spatial gradients (and so where the fine resolution of the method could be really useful). So it would be great to see the performances conditioned to cloudy conditions (maybe defined by some LWP thresholds). Also it would be interesting to see a scene (maybe a Stratocumulus or a convective scene from LES) with strong IWV gradients where the retrieval performances can be shown in detail.

Our simulations include many cloudy and precipitating scenes. To make this clearer in page 6 line 16 after, "In these maps there are around 80,000 simulations (we only used every 50 CloudSat measurements)." we will add: These simulations include, according to the CloudSat classification algorithm [Sassen and Wang, 2008] more than 10,000 clouds identified as cirrus and stratocumulus, around 500 identified as Cumulus, 7000 as nimbostratus, and 800 as deep convection. Further, these simulations include around 400 precipitating scenes with rain rates of up to 4.5 mm hr^{-1} according to the rain profile product [L'Ecuyer and Stephens, 2002].

The impacts of clouds can clearly be scene in Figure 7 which shows how the yield is affected under clear sky conditions versus all sky conditions. In page 9 line 4, We will add the following: The yield, however, improves substantially. For example, in the tropics, for 20W of transmit power, the yield becomes better than 0.85 (as opposed to better than 0.7) and for 50W become better than 0.95 (as opposed to better than 0.8). *This yield improvement under clear sky cases is due to the lack of the attenuation burden impose by hydrometeors.*

At this point we will add the following figure:

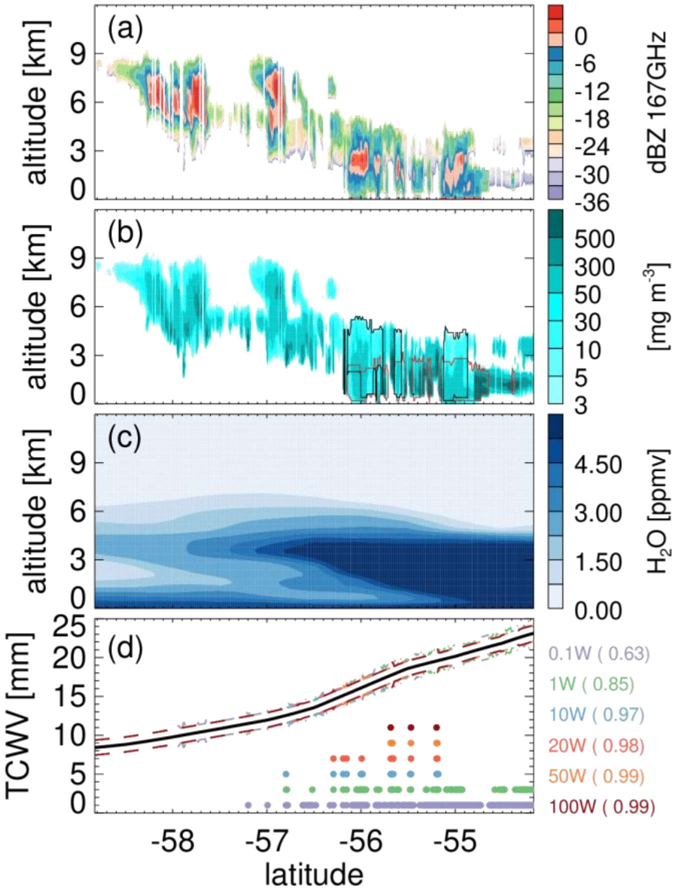

With the accompanying text: To further highlight that this technique will work under cloudy and precipitating conditions, Figure 8 shows a cross section of CloudSat-driven simulations over the Southern Ocean. This cross section consists of 500 CloudSat profiles encompassing ice clouds, liquid clouds, rain, and snow. Yields in this cross section are similar to those shown in Figure 7 at around 55S for the all scenes zonal average yield.

This new figure will have the following caption: Cross section exemplifying the CloudSat-driven simulations (data from 1 January 2007 over the Southern Ocean). (a) Simulated CloudSat-driven radar reflectivity at 167 GHz. (b) CloudSat retrieved total (IWC+LWC+rain+snow) hydrometeor water content. Black and red lines delimit areas where snow and rain were detected. (c) ECMWF-aux water vapor. (d) Total column water vapor (black solid line) as well as the retrieval precision (dashed lines) for different transmit powers and locations where at least one of the radar pulses was attenuated beneath the noise floor. Yield values for each simulated transmit powers are given by the numbers in brackets.

We did not use LWP because it breaks down under rainy condition where the CWC-RO algorithm fails. But we believe panel (b) shows clearly the hydrometeor burden.

Further, to emphasize that the *clear sky* systematic uncertainty (section 5.2) is really talking about cloudy and precipitating scenes we will change its name to “Clouds and precipitation errors” and the figure legend to “Cloud and Precip”.

To emphasis that the method will work in cloud and precipitation regions, the explanation of the systematic errors will be expanded to (page 10 line 7): As shown in Figure 8, most of the potential systematic uncertainties are lower than 0.5 mm, *including those uncertainties accounting for the extra attenuation impose by clouds and precipitation (as long as they do not attenuate completely the radar pulses)*. The exception are the errors associated with H_2O 183 GHz line width which could be as big as 1.4 mm…

Sassen, K., and Z. Wang, (2008) Classifying clouds around the globe with the CloudSat radar: 1-year of results, Geophys. Res. Lett., 35, L04805, doi:10.1029/2007GL032591

L’Ecuyer, T. S., and G. L. Stephens, 2002: An estimation-based precipitation retrieval algorithm for attenuating radars., J. Appl. Meteor., 41, 272-285.

2) Just to give an idea to the reader it would be good to know the single-pulse sensitivity for the radar specs tabulated in Tab.1. I expect 30 dB difference between the different powers? Is that correct? Is there any issue with the dynamic range of the surface reflectivity measurements?

We will add to table 1 the minimum detectable dB(s_0T^2) for each of the transmit power, the new line will say:

Minimum detectable[b] dB(s_0T^2) -18, -28, -38, -41, -45, -48.

[b] for each of the transmit powers considered, respectively.

We do not really know what the reviewer means by dynamic range of the surface reflectivity, it is precisely that range, the difference between 167 and 174.8 return the signal that we are exploiting to retrieve total column water vapor.

3) For Multiple scattering you state: “In all scenarios simulated here, the surface return dwarfed the multiple-scattered component of clouds and rain.” Well I am sure this is true everywhere but in deep convection. CloudSat surface return sometime is indeed dwarfed by multiple scattering in deep convection (several examples are provided in literature, e.g. Battaglia and Simmer, IEEE TRANSACTIONS ON GEOSCIENCE AND REMOTE SENSING,VOL. 46, NO. 6, JUNE 2008) I am sure that, when increasing the frequency, such instances will be more. It would be good this is quantified (maybe having a scene like suggested at 1) could help). Also what do the authors mean with “coarse” resolution of Cloudsat hydrometeors ? (I am still confused why the authors need to under-sample Cloudsat (computational time?)

The multiple scattering discussion on page 10 line 11 will be change to: In all scenarios *simulated here*, the surface return dwarfed the multiple-scattered component of clouds and rain. That is, the systematic uncertainty induced by ignoring multiple scattering effects was negligible, because the screening of the precipitating scenes (disregarding profiles which had any negative values) screened out those scenarios where multiple scattering was present. However, we do not anticipate that multiple scattering will be a problem, because according to Battaglia et al 2008, 80% of the rainy profiles can be accurately modeled assuming a single scattering approximation, and, further, in the order 20% of the cases, the strong hydrometeor burden will hinder the surface return.

We do under-sample CloudSat to save computational time, this will be stated clearer. In page 5 line 14, after the sentence “Note that, to decrease the number of calculations we subsample these fields, we only used one out of 50 CloudSat measurement.”, we will add: In other words, we under-sample CloudSat to save computational time.

Battaglia et al (2008), Identifying multiple-scattering-affected profiles in CloudSat observations over the oceans, doi: 10.1029/2008JD009960

Minor comments:
1) In the abstract I do not think that the authors actually mean “pulses will reach the surface” (for radar the pulses must also go back to the receiver to be detected!)

The reviewer is absolutely correct, we will change to: …both pulses will be detected with a signal to noise ratio > 1 at least 70% …

In page 8 line 25 where we define yield, the sentence will also be changed to: number of times surface reflections at both frequencies are detected with an SNR > 1 divided by the total number of simulations.

2) Sect.3: not clear what scattering model has been used for ice.

As mention in line 5 of page 5 (first paragraph of that section), “we use Mie scattering theory assuming spherical solid hydrometeors”, that is, we evaluate ice, liquid cloud particles, rain and snow using Mie theory. If the reviewer is asking for the particle size distribution that is given in table 2. Currently (at the end of that paragraph) it just states, More details can be found in Table 2. To make it clearer, this last sentence will be changed to: More details, *such as the dielectric constants and the particle size distributions used*, can be found in Table 2.

3) Sect.3: “we only used every 50 CloudSat measurement” (you mean one out of 50?)

Yes, we mean one out of 50, the sentence will be changed to: Note that, to decrease the number of calculations (save computational time) we subsample these fields, we only used one out of 50 CloudSat measurement.

Reviewer 2

We note that the reviewer comments refer to a previous version of the document. Those comments were already addressed. See below:

General comments:

This manuscript described a feasibility study of a differential absorption radar operating near a water vapor absorption line (183 GHz) in measuring total column water vapor from space. The considered radar system combined two tones (167 & 174.8 GHz) near the vapor absorption line and had potential radar powers ranging from 0.1 to 100 W. The radar system performances including measurement approaches and environment conditions were numerically simulated based on basic radar principles and global CloudSat observed hydrometeor and ECMWF atmospheric temperature, pressure and humidity profiles. Various measurement sensitivities and uncertainties were simulated. Results showed that with 20 W radar transmitted power satisfied measurements could be obtained for both land and ocean areas. This kind of satellite measurements could potentially provide additional global water vapor observations, particularly over land, besides passive infrared and microwave vapor soundings over oceans. This study was straight forward, and the manuscript was basically written well.

Based on the importance of water vapor observations, especially over global rural land and polar regions, for weather and climate studies, and the general and specific comments listed below, a minor revision is recommended.

1. The authors should clarify certain simulation procedures in obtaining the simulated random and systematic errors of total column water vapor measurements. Were those errors obtained based on uncertainty parameterization like Eq. 6 or the detailed radar signal propagation processes? Did they simulated the processes of the radar signal generation, transferring through the atmosphere, and reflecting at the surface with all adequate noise and uncertainties added in individual parts of the signal propagation processes? For example, when passing through atmosphere, what turbulence was considered for radar signals?

We believe that this is well explained through the manuscript, in particular section 3 (radar instrument simulator). The first paragraph states: Radar returns are simulated using the radiometric model described in Millán et al. (2014) and Millán et al. (2016). In short, radar reflectivities are estimated using the time-dependent two-stream approximation (Hogan and Battaglia, 2008), gaseous absorption is evaluated using the clear sky forward model for the EOS Microwave Limb Sounder (Read et al., 2004), hydrometeors scattering properties are evaluated using Mie scattering theory (assuming spherical hydrometeors), and the surface cross section is calculated using a quasi-specular scattering model (Li et al., 2005) for the ocean surface.

Turbulent process occurring at scales smaller than the CloudSat foorprint were not included. We added: It is noted that non-uniformities within the beam at scales smaller than the CloudSat horizontal resolution are not included in these simulations. They will be better addressed using either high resolution ground-based data or high resolution atmospheric models in subsequent studies.

To clarify how we studied the impact of the measurement noise we added (in section 4) the following: Instrument noise is not added to any of these simulations because its impacts are studied through equation 16.

2. For the radar system considered, what was the swath of spaceborne radar? The NRCS of surfaces may drop with increased scanning angle quickly. Could it scan like the precipitation radar onboard TRMM satellite? A related question is the sampling rate (or revisit time period) for a particular location.
The instrument simulated does not perform any cross-track scanning. This is an important issue to consider, however one could interpret these nadir calculations in an off-nadir context by scaling the angle dependence of the radar cross section with the various transmit powers that we consider here.

Specific comments:

There are some editing issues throughout the manuscript. Thorough proof-reading is required.

1. Abstract, Line 14:, '.. a fractional yield better than 0.7'. It is not clear what exactly this 'yield' means here. The authors defined this at a very late stage.
The text was changed to: Results indicate that, using two radar tones at 167 and 174.8GHz with a transmit power of 20W ensures that both pulses will reach the surface at least 70% of the time in the tropics and more than 90% of the time outside the tropics, and that total column water vapor can be retrieved with a precision better than 1.3 mm.

2. Pg2, Line 8: add 'a' after 'using' Done

3. Pg2, Line 9: add 'for' before 'all surfaces' It would be better if change 'all surfaces' to 'all surface types' Done

4. Pg2, Line 22: The authors wrote: '…. absorption line, respectively…' It would improve the readability if moving the 'respectively' to the end of this statement. Done

5. Pg2, Line 25: It sounds like there are some issues with the assumption of '0.16 dBZ radar precision, and around a -30dBZ minimum detectability'. Could the authors provide details on these issues, please?
The text was changed to: However, both studies assumed a *constant* instrument error model, with a 0.16dBZ radar precision, and around a -30dBZ minimum detectable signal. Here we use a more realistic uncertainty model (described in section 2) that includes speckle noise. That is, that depends on the magnitude of the return power which in turn depends on the water vapor burden.

6. Section 2, pg 3 and 4: this part could be shortened because of many cited papers and previous studies.
We decided to leave it as is for completeness, that way the reader can understand the paper without having to read the cited papers.

7. Pg3, L14: add 'parameter' after 'where C is the radar system'. Done

8. Pg4, L1: No need to make subsection 2.1. All in Section 2 would be fine. Done

9. Pg4, L12 and 25: The authors used a 66-us chirped pulse. This is a pretty long pulse. How big are the sidelobes of the pulse returns after coherent integration (or correlator)? Could the radar backscatterers at different ranges affect each other? What is the impact of those sidelobes? For example, what is the potential bias these sidelobes could produce when rain drops are considered? We added the following sentence at the end of that paragraph: Despite the relatively long chirp time, we do not simulated any sidelobes because, as demonstrated by RainCube (a Ka-band 6U cubesat radar with a 166-us pulse length), through an optimal selection of pulse shape and digital processing, sidelobes can be suppressed to accurately measure the most relevant precipitation processes near the surface [Peral et al (2019)].

10. Pg4, L20: The authors mentioned NT value is, at least, 2. Is it possible for the designed radar system to transmit the two tones together? If yes, what is the potential of cross-talks? If not, provide reasons besides cross-talks due to transmission and amplification.
Although theoretically it may be possible to transmit the two tones together, as simulated (and probably as implemented in a real instrument due to practicality) the radar system will not likely transmit the two tones together. Other cross-talk issues, if any, will have to be studied and corrected in the actual radar implementation, but in these simulations, they were not studied.

11. Pg4, L26: change ‘table’ to ‘Table’ for consistency. Also, please check other places such as line 7 in page 5.
Done

12. Fig. 1: Need enlarge the symbols of half circle and triangle. They are hard to read now. Done

13. Pg5, L14: What was the cited reference ‘Partin 2007’ exactly? A thesis or internal report? In either case, a link to the document is needed. Internal document, the reference was updated.

14. Pg5, L16: For radar operation frequencies of 167 and 174.8 GHz, could the authors let readers know how big the atmospheric gaseous attenuations at these frequencies are for some typical clear atmospheric profiles such as those with total column water vapor values of 35, 45 and 55 mm? What are the percentages of vapor attenuations on the totals?

We included a new figure:

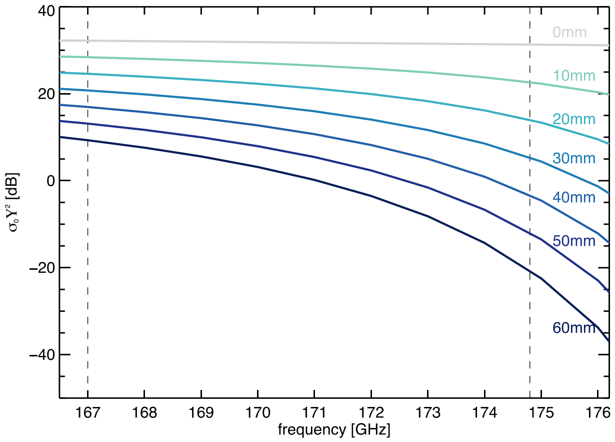

At the end of that paragraph we added: As examples of this burden, Figure 2 shows the spectral variation of the surface return for different total column water vapor burdens under clear sky conditions. The spectral contrast between 174.8 and 167GHz varies from 0.1dB for no water vapor to 31dB for 60mm of total column water vapor.

15. Pg5, L18 to 21: The study used two vapor profiles: wet and dry. It seems that the dry profile was not for zero vapor amount. Could the authors let readers know what the total column water vapor values were used in the simulation for wet and dry conditions? Also, how about other meteorological conditions such as the surface temperatures?
We added the following: (with 44 and 4mm of total column water vapor burden and 298 and 257K surface temperature, respectively)

16. Fig. 3: the colors in the figure were not easy to read due to inconsistency from cold to warm colors. The authors need change the color code.
We changed the colorbar for panels b and c (the panels showing the simulated CloudSat-driven effective surface cross-section for both frequencies). The colorbars for a and d are the same (but reverse or inconsistent as the reviewer points out) on *purpose* to highlight the similarities between the total column water vapor (panel a) and the difference between the two surface cross sections (panel d).

17. Pg6, L5 to 8: only 4 panels were shown. Please check this statement. Also, this statement may be too complicated and should be split into shorter sentences.

The statement was broken into 3 sentences (and the number of panels was corrected): The top panel is an 8-day average (January 1-8, 2007) of the CloudSat ECMWF-aux total column water vapor to show the context of the simulations. The next two panels show the average effective surface cross section, that is sigma0 at 167 and 174.8GHz. Lastly, the bottom panel shows the difference between the 174.8 and 167GHz simulations.

18. Eq. 17: Please provide references or a brief derivation to obtain this equation. Was the uncertainty used in the manuscript a variance or mean square error? What assumptions did the authors used in deriving this equation? This was confusing since it was not clear if the means or bias errors were included.

In the manuscript we added after that equation: which is simply the propagation of the individual errors of Pr(v2) and Pr(v1).

19. Pg7, L8: no need of the subsection 4.1. Done

20. Pg7, L15: '…. also provided by CloudSat.' Did the authors mean '… also provided by CloudSat-ECMWF product.'

Yes, It was changed to that.

21. Pg7, L17: *Wi* was a water vapor state variable. Readers expected it to be a vector for the water vapor profile. However, the iteration parameter ⍰1 − _*Wi+1* / *Wi* ⍰ _made it looked like a scaler. Was this value the total column water vapor? Please clarify this.

As specified in line 1 of page 7 (of the original manuscript): the shape of the assumed water vapor profile does not change during the retrieval, it is simply scaled according to the total column water vapor retrieved.

22. Pg7, L19 to 24 and Eqs. 19 and 20: Were instrument and measurement noises added when calculating the simulated radar returns? No, measurement noise is studied through equation 16 as it is often used when doing this type of studies. We could equivalently add the noise to the observed radar powers however it will not change any conclusions. The following sentence was added: Instrument noise is not added to any of these simulations because its impacts are studied through equation 16.

23. Pg8, L2: The authors mentioned precision here. Could the authors clarify if the retrievals had bias errors when only instrument and measurement noises were used? Many factors could introduce biases. For example, as mentioned previously, sidelobes could cause bias errors. If the answer is yes, how small or big are these biases?

No bias errors were investigated in this paper. Those biases are diagnosed using the mean value returned by an *actual* retrieval versus the *truth state* (given by in-situ measurements for instance). Those biases will vary depending on the actual retrieval scheme implemented, number of iterations, linearization profile, temperature and pressure used, etc, and hence not included in this study. The purpose of this study is to evaluate the possible precision and systematic biases and those ones, should not vary depending on the retrieval specifics.

24. Pg8, L4: '.. the impact of not knowing of temperature and pressure by using climatological values' How could this happen? People would think the authors or users of the spaceborne radar measurements should have products of numerical weather forecasts, assimilations and/or analyses of these temperature and pressure profiles? It is understandable to have certain uncertainties (or random and bias errors) associated with these modelled values, but it seems to pretty extreme to think without information on these values during environmental science satellite operations.

The reviewer is correct, in any retrieval scheme products of numerical weather forecast will be used as part of the retrieval. However, we used climatological values versus reanalysis values to study the *worst possible* impact of the uncertainties (as the reviewer also points out) of the modelled values. We changed that phrase to: … the impact of not knowing *precisely* the temperature and pressure …

Further, in the bullet describing these errors we added: Simply, these errors evaluate the worst possible impact of not knowing precisely the temperature and pressure.

25. Pg8, L15 to 17: Could the authors move the discussion on Fig 5 (SNR) after Fig. 4 discussions. That is, move these lines to the end of line 21.

After consideration, we believe that the text as is reads better, since the discussion of Figure 5 ties directly with: Further increasing the transmit power does little to improve the precision, because as we noted in section 2.1, in high SNR regimes, the fractional error in the measurement is largely determined by the number of uncorrelated pulses used.

26. Pg8, L18: The authors defined 'yield' here. For increasing readability, it should be defined much earlier when the first time it was used. The text in the abstract was changed, now, yield is defined immediately after its first mention.

27. Pg8, L19 and 20: change the words 'used before' to 'as those shown in left panels' Done

28. Pg9, L9: define 'pT'. We added (pressure-temperature)

29. Pg9, L25 and 26: The authors cited Meshkov (2006). The reference showed that this was a thesis. There was an article with the same title by Meshkov and De Lucia (2005). Were the essential contents of these two articles the same? If yes, the authors should cite the latter because of easier to obtain for readers.

We changed the citation to the article as recommended

30. End of pg9 and beginning of pg10: The authors found that potentially current uncertainties (4%) in the line width of the water vapor absorption line could cause about 1.4 mm total column water vapor bias errors. For this kind of significant systematic errors, can calibration and validation of the measurements of the instrument or even using an airborne radar at the frequencies considered over tropical regions or during midlatitude humid summer periods identify the bias and correct this potential systematic error? From random error analysis, it seems possible with long enough averages. If yes, the authors should make some comments and explanations, especially at the summery, on this, which would increase the feasibility of the instrument.

We added the following text: However, this type of bias should be easily corrected during a validation campaign since all retrievals will be off by the same *constant* amount.

Assessment of global total column water vapor sounding using a spaceborne differential absorption radar

Luis Millán[1], Richard Roy[1], and Matthew Lebsock[1]

[1]Jet Propulsion Laboratory, California Institute of Technology, Pasadena, California, USA

Correspondence: L. Millán (lmillan@jpl.nasa.gov)

Abstract.

The feasibility of using a differential absorption radar (DAR) to retrieve total column water vapor from space is investigated. DAR combines at least two radar tones near an absorption line, in this case a water vapor line, to measure humidity information from the differential absorption "on" and "off" the line. From a spaceborne platform, DAR can be used to retrieve total column water vapor by measuring the differential reflection from the Earth's Surface. We assess the expected precision, yield, and potential biases of retrieved total column water vapor values by applying an end-to-end radar instrument simulator to near-global weather analysis fields collocated with CloudSat measurements. The approach allows us to characterize the DAR performance across a globally representative dataset of atmospheric conditions including clouds and precipitation as well as different surface types.

We assume a hypothetical spaceborne G-band radar with pulse compression orbiting the earth at 405 km with a 1 m antenna, equivalent to a footprint diameter of 850 m, and 500 m horizontal integration. The simulations include the scattering effects of rain, snow, as well as liquid and ice clouds, spectroscopic uncertainties, and uncertainties due to the initial assumed water vapor profile. Results indicate that, using two radar tones at 167 and 174.8 GHz with a transmit power of 20 W ensures that both pulses will be detected with a signal to noise ratio greater than 1 at least 70% of the time in the tropics and more than 90% of the time outside the tropics, and that total column water vapor can be retrieved with a precision better than 1.3 mm.

1 Introduction

Water vapor is one of the most important gases in the Earth atmosphere. Its relevance has led to the development of several techniques for measuring its vertical distribution as well as the vertically integrated atmospheric water vapor content, which is often referred to as precipitable water, total water vapor, integrated water vapor, integrated precipitable water vapor or total column water vapor. The Global Climate Observing System has highlighted the utility of total column water vapor observations, declaring it as an essential climate variable (GCOS-ECV, 2020), which the World Meteorological Organization defines as a physical, chemical, or biological variable that critically contributes to the characterization of Earth's climate.

Passive satellite total column water vapor retrievals typically use instruments that measure in the visible (e.g., Lang et al., 2007; Wang et al., 2014), near-infrared (e.g., Lindstrot et al., 2012; Diedrich et al., 2015; Nelson et al., 2016), infrared (e.g., Pougatchev et al., 2009; Bedka et al., 2010), and microwave spectral regions (e.g., Schluessel and Emery, 1990; Wentz, 1997).

However, each spectral region has its limitations: Visible and near-infrared measurements are limited to cloud-free daytime regions and to land areas where the relatively bright surface reflection increases the signal compared to the dark ocean surfaces; infrared and microwave measurements can operate only over ice-free oceans, where the surface emissivity is well characterized. Additionally, infrared measurements are not possible in the presence of clouds or rain.

This study explores the feasibility of using a differential absorption radar (DAR) to remotely measure total column water vapor under all sky conditions, for all surfaces types and during day and night. The DAR technique is analogous to the differential absorption lidar (DIAL) technique (e.g., Schotland, 1966; Browell et al., 1979; Wulfmeyer and Walther, 2001), but operates in the microwave or millimeter-wave regime. In essence, the difference between the radar reflectivity at two nearby frequencies, “on” and “off” an absorption line, can be related to the amount of absorbing gas between the radar and the scattering target, which in this case is the Earth surface.

Prior studies have shown that the DAR technique can be used to derive water vapor profiles using three frequencies around 22 GHz (Meneghini et al., 2005), two frequencies at around 10 and 94 GHz (Tian et al., 2007) or at 2.8 and 35 GHz (Ellis and Vivekanandan, 2010). However, these studies require distinct radar transmitters for each frequency, which complicates the DAR measurement due to independent system calibration and beam overlap issues. Lebsock et al. (2015), Millán et al. (2016) and Battaglia and Kollias (2019) explored the feasibility of water vapor profiling with a narrow-band transmitter on the wings of the 183 GHz water vapor line, in which case the DAR measurement can be made with a single transceiver, greatly simplifying the measurement interpretation.

With respect to remotely measuring total column water vapor, Lebsock et al. (2015) and Millán et al. (2016) assessed the feasibility of using two frequencies near the 183 GHz water absorption line, using large eddy simulations and global cloud observations from CloudSat (Stephens et al., 2002), respectively. These studies concluded that the DAR technique could provide nearly spatially continuous observations of total column water vapor, even under rainy conditions. However, both studies assumed a *constant* instrument error model, with a 0.16 dBZ radar precision, and around a -30dBZ minimum detectable signal. Here we use a more realistic uncertainty model (described in section 2) that includes speckle noise. That is, that depends on the magnitude of the return power which in turn depends on the water vapor burden. Furthermore, their simulations explored frequencies prohibited by the Federal Communications Commission for space-borne transmission.

Here, we assume a frequency-chirp, pulsed radar system, similar to the proof of concept instrument described by Cooper et al. (2018) and by Roy et al. (2018). Currently, a similar airborne radar operating near 170 GHz is being developed and has recently been validated during a ground-based deployment (Roy et al., 2019). The motivation of this study is to investigate the transmit power necessary to achieve close to global total column water vapor measurements from a space platform given realistic instrument and orbital parameters, and using frequencies that could be available for space transmission.

2 Differential absorption radar theory

It has been shown (Lebsock et al., 2015; Millán et al., 2016), that the ratio of two surface returns can be used to estimate the total column water vapor. Nevertheless, for completeness, a description of the radar theory is summarized here. Neglecting multiple scattering, the surface return power measured by a monostatic radar which transmits a power P_{T} at a given frequency ν is given by,

$$P_{\mathrm{R}}(\nu) = \frac{P_{\mathrm{T}}(\nu)G(\nu)^2\lambda^2\Omega(\nu)}{(4\pi)^3 r^2}\Upsilon^2(\nu)\sigma_0(\nu) \tag{1}$$

where $G(\nu)$ is the antenna gain, r is the distance to the surface, $\Omega(\nu)$ is the integral of the normalized two-way antenna pattern, $\sigma_0(\nu)$ is the normalized surface cross section. $\Upsilon^2(\nu)$ is the two-way transmission given by,

$$\Upsilon^2(\nu) = \exp\left(-2\int\limits_0^r \left[\sigma_{\mathrm{gas}}(\nu,r') + \sigma_{\mathrm{Pext}}(\nu,r')\right]\mathrm{d}r'\right) \tag{2}$$

where $\sigma_{\mathrm{gas}}(\nu,r)$ represents the gaseous absorption coefficient and $\sigma_{\mathrm{Pext}}(\nu,r)$ the particulate extinction (the sum of absorption and scattering) coefficient along the radar path.

If two radar tones are measured simultaneously, the ratio of two surface returns can be expressed as,

$$\frac{P_{\mathrm{R}}(\nu_2)}{P_{\mathrm{R}}(\nu_1)} = \frac{C(\nu_2)}{C(\nu_1)}\frac{\Upsilon^2(\nu_2)}{\Upsilon^2(\nu_1)}\frac{\sigma_0(\nu_2)}{\sigma_0(\nu_1)} \tag{3}$$

where $C(\nu)$ is the radar system parameter given by the first term of equation 1, that is, $\frac{P_{\mathrm{T}}(\nu)G(\nu)^2\lambda^2\Omega(\nu)}{(4\pi)^3 r^2}$.

Assuming that the frequency dependence of $\sigma_{\mathrm{Pext}}(\nu,r)$ and $\sigma_0(\nu)$ is small relative to that of $\sigma_{\mathrm{gas}}(\nu,r)$, this equation becomes

$$\frac{P_{\mathrm{R}}(\nu_2)}{P_{\mathrm{R}}(\nu_1)} = \frac{C(\nu_2)}{C(\nu_1)}\exp\left(-2\int\limits_0^r \left[\sigma_{\mathrm{gas}}(\nu_2,r') - \sigma_{\mathrm{gas}}(\nu_1,r')\right]\mathrm{d}r'\right) \tag{4}$$

which can be rewritten as,

$$\frac{P_{\mathrm{R}}(\nu_2)}{P_{\mathrm{R}}(\nu_1)} = \frac{C(\nu_2)}{C(\nu_1)}\exp\left(-2\int\limits_0^r \rho(r')\sum_i v_i(r')\left[\kappa_i(\nu_2,r') - \kappa_i(\nu_1,r')\right]\mathrm{d}r'\right) \tag{5}$$

where $\rho(r)$ is the air density and the sum is over all the absorbers with mass extinction cross section $\kappa_i(\nu,r)$ and volume mixing ratio $v_i(r)$. If the radar tones are close to a strong absorption line, the associated gas dominates the absorption. For example, absorption due to water vapor dominates the atmospheric attenuation near 183 GHz. In that scenario, the only unknowns remaining are pressure, temperature and water vapor mixing ratio. It follows that assuming a temperature and pressure profile (for example, from reanalysis fields or a climatology), and a water vapor profile shape, it should be possible to retrieve total column water vapor from the ratio of two surface returns. The uncertainties associated with these assumed profiles will be discussed in section 5.2.

To explore the capabilities of this technique, the radar reflectivity uncertainty needs to be properly simulated. Here we assume a moving satellite platform with velocity V and antenna diameter D. Following Roy et al. (2018) and Roy et al. (2019), the uncertainty in the received power (see equation 1), assuming decorrelated pulses, is given by

$$\Delta P_{\mathrm{R}}(\nu)^2 = \frac{P_{\mathrm{R}}(\nu)^2}{N_p} + \frac{2P_{\mathrm{N}}P_{\mathrm{R}}(\nu)}{N_p} + \frac{2P_{\mathrm{N}}^2}{N_p} \tag{6}$$

where N_p is the number of pulses used in each measurement of $P_\mathrm{R}(\nu)$. The first term is due to speckle noise, the second term is known as Townes noise (i.e., Townes and Geschwind, 1948; Pearson et al., 2008), and the last term is due to the instrument thermal noise P_N. Speckle noise can be understood as the variation in backscatter from randomly distributed scatterers causing interference effects in the coherent measurement of the total returned electric field. In simple terms, Townes noise is due to the cross term of the sum of the signal and noise voltages. The instrument thermal noise is determined by

$$P_\mathrm{N} = \frac{k_b T_\mathrm{sys}}{\tau} \tag{7}$$

where k_b is the Boltzmann constant, T_sys is the system noise temperature, and τ is the chirp time which we fix according to the relation given by (Walsh, 1982),

$$\tau = \frac{D}{2V} \tag{8}$$

which ensures that sequential pulses are decorrelated.

The number of pulses is then determined by

$$N_p = \varsigma \frac{T}{\tau} \tag{9}$$

where ς is the duty cycle, assumed to be 0.25 using a chirped pulse, and T is the total integration time available for each radar tone, estimated using,

$$T = \frac{\Delta L}{V N_T} \tag{10}$$

where ΔL is the desired along-track horizontal resolution and N_T is the number of radar tones (e.g., at least two, for the online and the offline tones).

In this study we assume a 405 km orbit, a 1 m antenna diameter, radar tones at 167 and 174.8 GHz, a system temperature of 1800 K, a desired horizontal integration of 500 m, and transmit powers varying from 0.1 to 100 W. These assumptions result in a footprint diameter of ~850 m, a chirp time of 66μs, a total incoherent integration time per tone of 33 ms and 125 number of pulses. These radar characteristics are listed in Table 1 (which also includes the symbols used throughout this study). Further, we define the minimum detectable signal to be $P_\mathrm{R}(\nu) = P_\mathrm{N}$ (i.e. where a single pulse signal-to-noise ratio (SNR) is equal to 1). This determines the sensitivity of the DAR measurement system. Despite the relatively long chirp time, we do not simulated any sidelobes because, as demonstrated by RainCube (a Ka-band 6U cubesat radar with a 166μs pulse length), through an optimal selection of pulse shape and digital processing, sidelobes can be suppressed to accurately measure the most relevant precipitation processes near the surface (Peral et al., 2019).

The Earth's surface is a bright target, meaning that the SNR should be large. In this scenario, $P_\mathrm{R}(\nu)$ is generally much larger than P_N and the last 2 terms of equation 6 (the contributions from the Townes noise and the instrument noise) are small. Thus, in high-SNR regimes the fractional uncertainty in the received power simply becomes $1/\sqrt{N_p}$.

3 Radar Instrument Simulator

Radar returns are simulated using the radiometric model described in Millán et al. (2014) and Millán et al. (2016). In short, radar reflectivities are estimated using the time-dependent two-stream approximation (Hogan and Battaglia, 2008), gaseous absorption is evaluated using the clear sky forward model for the EOS Microwave Limb Sounder (Read et al., 2004), hydrometeors scattering properties are evaluated using Mie scattering theory (assuming spherical solid hydrometeors), and the surface cross section is calculated using a quasi-specular scattering model (Li et al., 2005) for the ocean surface. More details, such as the dielectric constants and the particle size distributions used, can be found in Table 2.

The hydrometeor fields used in this study are supplied by cloud/rain profiles observed by CloudSat. CloudSat is a NASA satellite carrying a 94 GHz profiling radar sensitive to both cloud and precipitation particles (Stephens et al., 2002). CloudSat retrievals provide the hydrometeor information while spatially and temporally interpolated weather analysis provides the meteorological conditions. In particular, rain and snow profiles are taken from the 2C-RAINPROFILE (Lebsock and L'Ecuyer, 2011) products and liquid water content (LWC) and ice water content (IWC) from the 2B-CWCRO R04 (Austin and Stephens, 2001; Austin et al., 2009). Temperature, pressure, and water vapor are taken from the European Centre for Medium-Range Weather Forecasts auxiliary (ECMWF-aux) products (Cronk and Partain, 2017). Note that, to decrease the number of calculations we subsample these fields, we only used one out of every 50 CloudSat measurement. In other words, we under-sample CloudSat to save computational time. It is noted that non-uniformities within the beam at scales smaller than the CloudSat horizontal resolution are not included in these simulations. They will be better addressed using either high resolution ground-based data or high resolution atmospheric models in subsequent studies.

Figure 1 shows an example simulation at 167 and 174.8 GHz, which are the two frequencies used throughout this study. These frequencies are the extreme frequency values achievable due to international transmission restrictions (NTIA, 2015). The observed scene is heavily overcast with snow aloft and rain beneath the freezing level. The simulation is repeated for two distinct water vapor burdens; a wet atmosphere as estimated from the weather analysis and a hypothetical dry atmosphere (with 44 and 4 mm of total column water vapor burden and 298 and 257 K surface temperature, respectively). As expected, the dry atmosphere simulations show considerably less attenuation, but nevertheless, the impact of the water vapor burden is clearly visible in the extra attenuation experienced by the 174.8 GHz radar tone compared to 167 GHz. As examples of this burden, Figure 2 shows the spectral variation of the surface return for different total column water vapor burdens under clear sky conditions. The spectral contrast between 174.8 and 167 GHz varies from 0.1dB for no water vapor to 31 dB for 60 mm of total column water vapor.

We use a quasi-specular surface backscatter model over the oceans (Li et al., 2005) assuming monthly climatological values derived from the ERA-Interim reanalysis for near surface wind speed and sea surface temperature (Dee et al., 2011). Over land surfaces there are no empirical models for the radar cross section at these frequencies. Therefore we use the observed cross sections from CloudSat to scale the ocean frequency dependence of the Li et al. (2005) model as follows,

$$\sigma_0(\nu)' = \sigma_0^c(\nu_{94})\psi \tag{11}$$

where $\sigma_0(\nu)'$ is the modified surface cross section at a given frequency, $\sigma_0^c(\nu_{94})$ is the measured CloudSat cross section, and ψ is the ratio between the cross section simulated by the ocean back scatter model at the desired frequency and the cross section simulated by the ocean back scatter model at 94 GHz (CloudSat's frequency). Under most wind, temperature, and salinity conditions, ψ is ∼0.78 at 167 GHz and ∼0.76 at 174.8 GHz. We emphasize that this method is ad-hoc and does not properly account for the differences in the spectral dependence of the reflectance properties of land surfaces versus water surfaces. Nonetheless it allows us to examine the feasibility of the remote sensing method. As an example, Figure 3 shows maps of the measured CloudSat cross section as well as the modeled surface cross section at 167 GHz for the simulations used in this study. As explained by Haynes et al. (2009), $\sigma_0^c(\nu_{94})$ displays large spatial variability over land, where $\sigma_0(\nu)$ depends on vegetation, soil moisture, surface slope, snow cover, etc; as opposed to over the oceans where it mostly depends upon the wind speed through its effect on the surface slope distribution. Although equation 11 approximates the frequency dependence of land surface backscatter using an ocean model, the land-specific frequency dependence is minimal and should have only a minor effects on results. The impact of uncertainties on $\sigma_0(\nu)$ will be discussed in section 5.2.

Figure 4 shows maps of the DAR simulations used in this study. The top panel is an 8-day average (January 1-8, 2007) of the CloudSat ECMWF-aux total column water vapor to show the context of the simulations. The next two panels show the average effective surface cross section, that is $\sigma_0(\nu)\Upsilon(\nu)^2$, at 167 and 174.8 GHz. Lastly, the bottom panel shows the difference between the 174.8 and 167 GHz simulations. Note that the simulations also include the hydrometeor burden, that is, the IWC, LWC, rain and snow found on each Cloudsat profile, which in principle is frequency-dependent. In these maps there are around 80,000 simulations (we only used every 50 CloudSat measurements). These simulations include, according to the CloudSat classification algorithm (Sassen and Wang, 2008) more than 10,000 clouds identified as cirrus and stratocumulus, around 500 identified as cumulus, 7000 as nimbostratus, and 800 as deep convection. Further, these simulations include around 400 precipitating scenes with rain rates of up to 4.5 mm hr^{-1} according to the rain profile product (L'Ecuyer and Stephens, 2002).

As shown, the impact of the water vapor burden can be seen at both radar tones, however, at 174.8 GHz the radar signal has been considerably more attenuated than at 167 GHz (which is further from the absorption line). Furthermore, the effective cross section difference (174.8 - 167 GHz), equivalent to the surface radar power ratios, is clearly strongly correlated with the total column water vapor field.

4 Retrieval Methodology

The aims of this study are to (1) quantify the uncertainties in DAR retrievals of total column water vapor and (2) to explore the trade-offs between radar transmit power and sampling of the Earth's real world meteorological variability. To accomplish this goal we performed end-to-end retrieval simulations. The retrieval algorithm used is,

$$w_{i+1} = w_i + \frac{\partial \hat{y}(w,\mathbf{b})}{\partial w}\left[y - \hat{y}(w_i,\mathbf{b})\right] \tag{12}$$

where the total column water vapor, w_i, is computed by suitably integrating the vertical water vapor profile $\mathbf{x}_i$, and y is determined by the ratios between surface radar returns at different frequencies, that is to say

$$y = \frac{P_{\mathrm{R}}(\nu_2)}{P_{\mathrm{R}}(\nu_1)} \tag{13}$$

and the simulated measurements, $\hat{y}(w_i, \mathbf{b})$, are given by,

$$\hat{y}(w_i, \mathbf{b}) = \frac{F_{\nu_2}(w_i, \mathbf{b})}{F_{\nu_1}(w_i, \mathbf{b})} \tag{14}$$

where F is the radar forward model described in section 3 and $\mathbf{b}$ is comprised of forward model parameters that influence the simulated radar observations but are not retrieved. For example,these include spectroscopic parameters, profiles of temperature, pressure, ice water content, liquid water content, rain or snow. The assumptions made in $\mathbf{b}$ contribute to the systematic errors in the estimates of the total column water vapor. In each iteration, $\partial\hat{y}(w, \mathbf{b})/\partial w$ is evaluated by finite differences by perturbing the entire water vapor profile, $\mathbf{x}_i$, by 1%. Lastly, after each iteration $\mathbf{x}_{i+1}$ is computed following,

$$\mathbf{x}_{i+1} = \frac{w_{i+1}}{w_i}\mathbf{x}_i \tag{15}$$

That is, the shape of the assumed water vapor profile does not change during the retrieval, it is simply scaled according to the total column water vapor retrieved.

The estimated precision (the error due to random noise affecting the instrument) in the retrieved total column water vapor, w, is given by,

$$\sigma_w^2 = \left[\frac{\partial\hat{y}(w, \mathbf{b})}{\partial w}\sigma_y\right]^2 \tag{16}$$

where σ_y is given by,

$$\sigma_y^2 = \left[\frac{P_{\mathrm{R}}(\nu_2)}{P_{\mathrm{R}}(\nu_1)}\sqrt{\left(\frac{\Delta P_{\mathrm{R}}(\nu_2)}{P_{\mathrm{R}}(\nu_2)}\right)^2 + \left(\frac{\Delta P_{\mathrm{R}}(\nu_1)}{P_{\mathrm{R}}(\nu_1)}\right)^2}\right]^2 \tag{17}$$

which is simply the propagation of combining the individual errors of $P_{\mathrm{R}}(\nu_2)$ and $P_{\mathrm{R}}(\nu_1)$.

To perform end-to-end retrievals, we first need to defined a set of conditions regarded as truth as well as the radar characteristics. As detailed in section 3, these conditions were taken from Cloudsat measurements (IWC, LWC, rain, snow, temperature and pressure) while the radar characteristics are listed in Table 1. With these atmospheric conditions and radar parameters, we compute synthetic radar returns to be used as measurements, that is, the synthetic radar returns are given by

$$P_{\mathrm{R}} = F(w_T, \mathbf{b_T}) \tag{18}$$

where w_T is the true water vapor state as provided by the CloudSat-ECMWF product, and where $\mathbf{b_T}$ represents the rest of the atmospheric state (temperature, pressure, and hydrometeor profiles) also provided by the CloudSat-ECMWF product.

These synthetic radar returns are then run through the retrieval algorithm. For the retrieved profile shape, $\mathbf{x_0}$, a water vapor profile taken from a ERA-Interim monthly climatology was used. The iterative procedure stops when $|1 - \frac{w_{i+1}}{w_i}|$ is lower than 0.05, which is normally achieved within 2 iterations.

During these retrievals we assume perfect knowledge of the forward model parameters, that is, the simulated radar returns used during the retrieval are given by,

$$\hat{P_{\mathrm{R}}} = F(w_i, \mathbf{b_T}) \tag{19}$$

or in other words, the only variable changing between y and $\hat{y}$ is the water vapor burden.

Sensitivity to assumed parameters is estimated using a perturbed set of synthetic radar returns following,

$$P'_{\mathrm{R}} = F(w_T, \mathbf{b}') \tag{20}$$

where $\mathbf{b}'$ represents the perturbed forward model parameter. Only one of the parameters is perturbed at a time; for instance, when computing the systematic uncertainty related to temperature, only the temperature values are perturbed, while the rest (IWC, LWC, rain, snow, particle size distributions, etc) are left unperturbed. Then, the retrieved total column water vapor using the perturbed measurements are compared to the retrieved values from an unperturbed run, i.e. using the measurements given by equation 18. The difference between the two retrieved total column water vapor is used a measure of the impact of a given systematic error source. Instrument noise is not added to any of these simulations because its impacts are studied through equation 16.

5 Results

First we will explore the precision, that is, the expected random error associated with the radar uncertainty described in section 2. Then we will explore potential systematic errors, such as the impact of not knowing the hydrometeor burden by assuming clear sky conditions throughout the forward model simulations, the impact of not knowing precisely the temperature and pressure by using climatological values, the impact of changing the initial assumed water vapor profile, the impact of the spectroscopy errors, and surface roughness uncertainties by using a constant value.

5.1 Precision

Figure 5-left shows maps of the total column water vapor precision (random error) assuming different transmit powers. White areas denote regions with no CloudSat measurements to initialize the simulations (i.e. the poles) or regions where the pulses (the simulated P_R's used in $\mathbf{y}$) are attenuated beneath the noise floor (i.e. the tropics when using 0.1 W of transmit power). As shown even with just a transmit power of 0.1 W, errors are better than 1.2 mm throughout the globe except at the tropics where the radar tones are completely attenuated. With a transmit power greater than 20 W errors are mostly below 1.2 mm everywhere except in active deep convective regions such as the maritime continent. Further increasing the transmit power does little to improve the precision, because as we noted in section 2, in high SNR regimes, the fractional error in the measurement is largely determined by the number of uncorrelated pulses used. Figure 6 shows the cumulative SNR histogram for the 174.8 GHz surface returns. As can be seen, most of the time, the SNR is higher than 10 even when using just 0.1 W. The SNR for the 167 GHz radar tone is slightly better since it experiences less water vapor attenuation.

Instead, increasing the transmit power improves the yield, that is, the number of times surface reflections at both frequencies are detected with a SNR greater than 1 divided by the total number of simulations. Figure 5-right shows fractional yield maps for the same transmit powers as those shown in left panels. Overall, even with only 0.1 W transmit power, the yield is better than 0.7 throughout most of the globe except at the tropics where the yield sharply drops to zero. The yield improves drastically when using at least 10 W.

To complement these maps, Figure 7 shows the random errors and the fractional yield zonal averages. Outside the tropics, that is polewards of 30^oS or 30^oN, regardless of transmit power, random errors are generally below 1.2 mm with fractional yields better than 0.7. With a transmit power of at least 10 W the random errors are below 1 mm and the fractional yield improves to better than 0.9. In the tropics, using at least 20 W, the random errors are mostly below 1.3 mm with fractional yields better than 0.7, improving to random errors mostly below 1.2 mm with fractional yields better than 0.8 when using at least 50 W. Under clear sky conditions, the random errors remain mostly the same. The yield, however, improves substantially. For example, in the tropics, for 20 W of transmit power, the yields becomes better than 0.85 (as opposed to better than 0.7) and for 50 W become better than 0.95 (as opposed to better than 0.8). This yield improvement under clear sky cases is due to the lack of the attenuation burden impose by hydrometeors.

To further highlight that this technique will work under cloudy and precipitating conditions, Figure 8 shows a cross section of CloudSat-driven simulations over the Southern Ocean. This cross section consists of 500 CloudSat profiles encompassing ice clouds, liquid clouds, rain, and snow. Yields in this cross section are similar to those shown in Figure 7 at around 55°S for the all scenes zonal average yield.

To date, passive microwave instruments have provided the benchmark for total column water vapor measurements. For example, the Advanced Microwave Scanning Radiometer (AMSR) instruments have an estimated error of $\sim$0.6 mm (Wentz and Meissner, 2000) for a native footprint of around 14 km by 8 km (Kawanishi et al., 2003). The precision of aggregated DAR total column water vapor measurements (the ones simulated here) matching such a footprint would be considerably better.

5.2 Systematic Uncertainties

Figure 9 shows zonal averages of eight potential systematic uncertainties sources. As explained in section 4, these systematic errors arise from the uncertainties in the ancillary knowledge used (including the spectroscopy uncertainties) throughout the retrievals. For example, as shown by equation 5 the uncertainties in the water vapor mass extinction cross section, $\kappa(\nu, r)$, will affect the estimated total column water vapor. Note that these systematic errors are independent of the transmit power as long as the surface return is not completely attenuated by the atmosphere. As such, these simulations were performed using 100 W to evaluate them under most conditions, that is, we use 100 W because it has the better yield. The systematic error sources studied here are explained below:

- pT (pressure-temperature) Climatology: Errors associated with using climatological pressure and temperature conditions throughout the forward model end-to-end simulated retrievals as opposed to using the actual pressure and temperature conditions. The climatological values correspond to January 2007 ERA-Interim monthly mean values for the 12 UT synoptic time. Simply, these errors evaluate the worst possible impact of not knowing precisely the temperature and pressure.

- Clouds and precipitation errors: Errors associated with assuming clear sky conditions throughout the end-to-end retrieval simulations as opposed to using the actual hydrometeors conditions. In other words, having no hydrometeor information to constrain the retrievals. Note that these error estimates evaluate the additional frequency dependent attenuation imposed by the hydrometeors. That is, it is assumed that the radar system is capable of identifying the surface return through coarse ranging capability.
- Assumed water vapor profile: Errors associated with using a different linearization water vapor profile in the end-to-end simulated retrievals. The assumed profiles are perturbed by up to 20% by layers. That is, we perturb the profile between 0-2, 2-4, 4-6, and 6-8 km individually and then aggregate the systematic uncertainty.
- Multiple scattering: Errors associated with simulating single scattering returns as opposed to multiple scattering ones.
- H_2O 183 GHz line strength: Error associated with perturbing the 183 GHz water vapor line strength by 0.25% following the uncertainty described by Pickett et al. (1998).
- H_2O 183 GHz line width: Error associated with perturbing the 183 GHz water vapor line width by 4% following Bauer et al. (1989) and Goyette and Lucia (1990).
- H_2O continuum: Error associated with perturbing the H_2O continuum by 10% following Meshkov and De Lucia (2005).
- O_2 and N_2 continuum: Errors associated with perturbing the O_2 and N_2O continuum by 10% following Meshkov and De Lucia (2005).
- Surface roughness: Errors associated with using a constant 12 ms^{-1} as opposed to a surface wind climatology.

As shown in Figure 9, all the potential systematic uncertainties are lower than 0.5 mm, including those uncertainties accounting for the extra attenuation impose by clouds and precipitation (as long as they do not attenuate completely the radar pulses). The exception are the errors associated with H_2O 183 GHz line width which could be as big as 1.4 mm. As expected, this uncertainty is approximately 4% of the total column water vapor because a H_2O line width perturbation mostly equates to perturbing the measurement, that is the ratio of the surface radar returns at different frequencies, by the same amount. However, this type of bias should be easily corrected during a validation campaign since all retrievals will be off by the same *constant* amount.

In all scenarios simulated here, the surface return dwarfed the multiple-scattered component of clouds and rain. That is, the systematic uncertainty induced by ignoring multiple scattering effects was negligible, because the screening of the precipitating scenes (disregarding profiles which had any negative values) screened out those scenarios where multiple scattering was present. However, we do not anticipate that multiple scattering will be a problem, because according to Battaglia et al. (2008), 80% of the rainy profiles can be accurately modeled assuming a single scattering approximation, and, further, in the order 20% of the cases, the strong hydrometeor burden will presumably hinder the surface return.

6 Summary

We have evaluated the precision, yield, and systematic uncertainties of a differential absorption radar to measure total column water vapor from space. This technique requires at least two radar tones near the 183 GHz water vapor absorption line ("on" and "off" the line) to infer the humidity burden between the radar and the surface. In this work, we used 167 and 174.8 GHz, the extremes of the frequency range of VIPR (Roy et al., 2019). Further, we assume an antenna diameter of 1 m, a horizontal integration of 500 m, an integration time of 33 ms, a system temperature of 1800 K, an orbit of 405 km, and transmit powers varying from 0.1 to 100 W.

We apply a radar instrument simulator to weather analysis fields colocated with CloudSat near-global measurements to simulate surface radar returns to be used as measurements in end-to-end retrievals. We use an iterative least-squares fit retrieval algorithm that allow us to quantify both the expected precision and the impact of potential systematic uncertainties upon the retrieved total column water vapor.

Systematic uncertainties related to the pressure and temperature, the hydrometeor burden, the initial guess, the water vapor line strength, the water vapor, O_2 and N_2 continuum, multiple scattering effects, and the magnitude of the surface winds could result in potential biases lower than 0.5 mm. Systematic uncertainties associated with the water vapor line width could be up to 1.4 mm. This approximately corresponds to 4% of the total column water vapor because a H_2O line width perturbation mostly equates to perturb the ratio of the surface radar returns by the same amount.

Precision and yield results can be summarized as follows:

- Outside the tropics, regardless of transmit power, random errors are generally below 1.2 mm with fractional yields better than 0.7. With a transmit power of at least 10 W the random errors are below 1 mm and the fractional yield improves to better than 0.9.
- In the tropics, using at least 20 W, the random errors are mostly below 1.3 mm with fractional yields better than 0.7, improving to mostly below 1.2 mm with fractional yields better than 0.8 when using at least 50 W.

These results suggest that at least 20 W of transmit power are needed to be able to measure total column water vapor globally with a reasonable yield. Output powers in the 10-100 W range would require additional research and development. DAR holds considerable potential as a technique to study the distribution of total column water vapor globally, that is, under most terrains and under most meteorological conditions, with considerably high horizontal resolution.

Data availability. The CloudSat dataset used in this manuscript can be found on the CloudSat data processing center website (http://www.cloudsat.cira.colostate.edu/order-data)

Author contributions. LFMV wrote the algorithm and carried out the analyses. RJR and MDL provided scientific expertise throughout all stages of the research.

Competing interests. There are no competing interests

Acknowledgements. The research was carried out at the Jet Propulsion Laboratory, California Institute of Technology, under a contract with the National Aeronautics and Space Administration. We thank Ken Cooper for his support throughout this research.

References

Abel, S. J. and Boutle, I. A.: An improved representation of the raindrop size distribution for single-moment microphysics schemes, Quarterly Journal of the Royal Meteorological Society, 138, 2151–2162, https://doi.org/10.1002/qj.1949, 2012.

Austin, R. T. and Stephens, G. L.: Retrieval of stratus cloud microphysical parameters using millimeter-wave radar and visible optical depth in preparation for CloudSat: 1. Algorithm formulation, Journal of Geophysical Research: Atmospheres, 106, 28 233–28 242, https://doi.org/10.1029/2000JD000293, 2001.

Austin, R. T., Heymsfield, A. J., and Stephens, G. L.: Retrieval of ice cloud microphysical parameters using the CloudSat millimeter-wave radar and temperature, Journal of Geophysical Research: Atmospheres, 114, https://doi.org/10.1029/2008JD010049, d00A23, 2009.

Battaglia, A. and Kollias, P.: Evaluation of differential absorption radars in the 183 GHz band for profiling water vapour in ice clouds, Atmospheric Measurement Techniques, 12, 3335–3349, https://doi.org/10.5194/amt-12-3335-2019, https://www.atmos-meas-tech.net/12/3335/2019/, 2019.

Battaglia, A., Haynes, J. M., L'Ecuyer, T., and Simmer, C.: Identifying multiple-scattering-affected profiles in CloudSat observations over the oceans, Journal of Geophysical Research, 113, https://doi.org/10.1029/2008jd009960, https://doi.org/10.1029/2008jd009960, 2008.

Bauer, A., Godon, M., Kheddar, M., and Hartmann, J.: Temperature and perturber dependences of water vapor line-broadening. Experiments at 183 GHz; calculations below 1000 GHz, Journal of Quantitative Spectroscopy and Radiative Transfer, 41, 49–54, https://doi.org/10.1016/0022-4073(89)90020-4, 1989.

Bedka, S., Knuteson, R., Revercomb, H., Tobin, D., and Turner, D.: An assessment of the absolute accuracy of the Atmospheric Infrared Sounder v5 precipitable water vapor product at tropical, midlatitude, and arctic ground-truth sites: September 2002 through August 2008, Journal of Geophysical Research, 115, https://doi.org/10.1029/2009jd013139, 2010.

Browell, E. V., Wilkerson, T. D., and Mcilrath, T. J.: Water vapor differential absorption lidar development and evaluation, Appl. Opt., 18, 3474–3483, https://doi.org/10.1364/AO.18.003474, 1979.

Cooper, K. B., Monje, R. R., Millán, L., Lebsock, M., Tanelli, S., Siles, J. V., Lee, C., and Brown, A.: Atmospheric Humidity Sounding Using Differential Absorption Radar Near 183 GHz, IEEE Geoscience and Remote Sensing Letters, pp. 1–5, https://doi.org/10.1109/lgrs.2017.2776078, 2018.

Cronk, H. and Partain, P.: CloudSat ECMWF-AUX Auxillary Data Product Process Description and Interface Control Document, Product Version: P_R05, http://www.cloudsat.cira.colostate.edu/sites/default/files/products/files/ECMWF-AUX_PDICD.P_R05.rev0_.pdf, 2017.

Dee, D. P., Uppala, S. M., Simmons, A. J., Berrisford, P., Poli, P., Kobayashi, S., Andrae, U., Balmaseda, M. A., Balsamo, G., Bauer, P., Bechtold, P., Beljaars, A. C. M., van de Berg, L., Bidlot, J., Bormann, N., Delsol, C., Dragani, R., Fuentes, M., Geer, A. J., Haimberger, L., Healy, S. B., Hersbach, H., Hólm, E. V., Isaksen, L., Kållberg, P., Köhler, M., Matricardi, M., McNally, A. P., Monge-Sanz, B. M., Morcrette, J.-J., Park, B.-K., Peubey, C., de Rosnay, P., Tavolato, C., Thépaut, J.-N., and Vitart, F.: The ERA-Interim reanalysis: configuration and performance of the data assimilation system, Quarterly Journal of the Royal Meteorological Society, 137, 553–597, https://doi.org/10.1002/qj.828, 2011.

Diedrich, H., Preusker, R., Lindstrot, R., and Fischer, J.: Retrieval of daytime total columnar water vapour from MODIS measurements over land surfaces, Atmospheric Measurement Techniques, 8, 823–836, https://doi.org/10.5194/amt-8-823-2015, 2015.

Ellis, S. M. and Vivekanandan, J.: Water vapor estimates using simultaneous dual-wavelength radar observations, Radio Science, 45, https://doi.org/10.1029/2009rs004280, 2010.

GCOS-ECV: Global Climate Observing System - Essential Climate Variable (accessed March 11, 2020), https://www.ncdc.noaa.gov/gosic/gcos-essential-climate-variable-ecv-data-access-matrix/gcos-atmosphere-upper-air-ecv-water-vapour, 2020.

Goyette, T. M. and Lucia, F. C. D.: The pressure broadening of the 31, 3-22, 0 transition of water between 80 and 600 K, Journal of Molecular Spectroscopy, 143, 346–358, https://doi.org/10.1016/0022-2852(91)90099-v, 1990.

Haynes, J. M., L'Ecuyer, T. S., Stephens, G. L., Miller, S. D., Mitrescu, C., Wood, N. B., and Tanelli, S.: Rainfall retrieval over the ocean with spaceborne W-band radar, Journal of Geophysical Research, 114, https://doi.org/10.1029/2008jd009973, 2009.

Hogan, R. J.: Multiscatter: a fast, approximate multiple scattering algorithm, 2013.

Hogan, R. J. and Battaglia, A.: Fast Lidar and Radar Multiple-Scattering Models. Part II: Wide-Angle Scattering Using the Time-Dependent Two-Stream Approximation, Journal of the Atmospheric Sciences, 65, 3636–3651, https://doi.org/10.1175/2008jas2643.1, 2008.

Hufford, G.: A model for the complex permittivity of ice at frequencies below 1 THz, International Journal of Infrared and Millimeter Waves, 12, 677–682, https://doi.org/10.1007/bf01008898, 1991.

Kawanishi, T., Sezai, T., Ito, Y., Imaoka, K., Takeshima, T., Ishido, Y., Shibata, A., Miura, M., Inahata, H., and Spencer, R.: The advanced microwave scanning radiometer for the earth observing system (AMSR-E), NASDA's contribution to the EOS for global energy and water cycle studies, IEEE Transactions on Geoscience and Remote Sensing, 41, 184–194, https://doi.org/10.1109/tgrs.2002.808331, https://doi.org/10.1109/tgrs.2002.808331, 2003.

Lang, R., Casadio, S., Maurellis, A. N., and Lawrence, M. G.: Evaluation of the GOME Water Vapor Climatology 1995–2002, Journal of Geophysical Research, 112, https://doi.org/10.1029/2006jd008246, 2007.

Lebsock, M. D. and L'Ecuyer, T. S.: The retrieval of warm rain from CloudSat, Journal of Geophysical Research: Atmospheres, 116, https://doi.org/10.1029/2011JD016076, d20209, 2011.

Lebsock, M. D., Suzuki, K., Millán, L. F., and Kalmus, P. M.: The feasibility of water vapor sounding of the cloudy boundary layer using a differential absorption radar technique, Atmospheric Measurement Techniques, 8, 3631–3645, https://doi.org/10.5194/amt-8-3631-2015, 2015.

L'Ecuyer, T. S. and Stephens, G. L.: An Estimation-Based Precipitation Retrieval Algorithm for Attenuating Radars, Journal of Applied Meteorology, 41, 272–285, https://doi.org/10.1175/1520-0450(2002)041<0272:aebpra>2.0.co;2, https://doi.org/10.1175/1520-0450(2002)041<0272:aebpra>2.0.co;2, 2002.

Li, L., Heymsfield, G. M., Tian, L., and Racette, P. E.: Measurements of Ocean Surface Backscattering Using an Airborne 94-GHz Cloud Radar Implication for Calibration of Airborne and Spaceborne W-Band Radars, Journal of Atmospheric and Oceanic Technology, 22, 1033–1045, https://doi.org/10.1175/jtech1722.1, 2005.

Liebe, H. J., Hufford, G. A., and Manabe, T.: A model for the complex permittivity of water at frequencies below 1 THz, Int J Infrared Milli Waves, 12, https://doi.org/10.1007/BF01008897, 1991.

Lindstrot, R., Preusker, R., Diedrich, H., Doppler, L., Bennartz, R., and Fischer, J.: 1D-Var retrieval of daytime total columnar water vapour from MERIS measurements, Atmospheric Measurement Techniques, 5, 631–646, https://doi.org/10.5194/amt-5-631-2012, 2012.

McFarquhar, G. M. and Heymsfield, A. J.: Parameterization of Tropical Cirrus Ice Crystal Size Distributions and Implications for Radiative Transfer: Results from CEPEX, J. Atmos. Sci., 54, 2187–2200, https://doi.org/10.1175/1520-0469(1997)054<2187:POTCIC>2.0.CO;2, 1997.

Meneghini, R., Liao, L., and Tian, L.: A Feasibility Study for Simultaneous Estimates of Water Vapor and Precipitation Parameters Using a Three-Frequency Radar, Journal of Applied Meteorology, 44, 1511–1525, https://doi.org/10.1175/jam2302.1, 2005.

Meshkov, A. I. and De Lucia, F. C.: Broadband absolute absorption measurements of atmospheric continua with millimeter wave cavity ring-down spectroscopy, Review of Scientific Instruments, 76, 083 103, https://doi.org/10.1063/1.1988027, https://doi.org/10.1063/1.1988027, 2005.

Millán, L., Lebsock, M., Livesey, N., Tanelli, S., and Stephens, G.: Differential absorption radar techniques: surface pressure, Atmospheric Measurement Techniques, 7, 3959–3970, https://doi.org/10.5194/amt-7-3959-2014, 2014.

Millán, L., Lebsock, M., Livesey, N., and Tanelli, S.: Differential absorption radar techniques: water vapor retrievals, Atmospheric Measurement Techniques, 9, 2633–2646, https://doi.org/10.5194/amt-9-2633-2016, 2016.

Nelson, R. R., Crisp, D., Ott, L. E., and O'Dell, C. W.: High-accuracy measurements of total column water vapor from the Orbiting Carbon Observatory-2, Geophysical Research Letters, 43, 12,261–12,269, https://doi.org/10.1002/2016GL071200, 2016.

NTIA: National Telecommunications and Information Administration: Manual of Regulations and Procedures for Federal Radio Frequency Management. (accessed March 3, 2020), https://www.ntia.doc.gov/page/2011/manual-regulations-and-procedures-federal-radio-frequency-management-redbook, 2015.

Pearson, J. C., Cooper, K., and Drouin, B. J.: Spectroscopic detection, fundamental limits and system considerations, in: 2008 33rd International Conference on Infrared, Millimeter and Terahertz Waves, IEEE, https://doi.org/10.1109/icimw.2008.4665839, 2008.

Peral, E., Tanelli, S., Statham, S., Joshi, S., Imken, T., Price, D., Sauder, J., Chahat, N., and Williams, A.: RainCube: the first ever radar measurements from a CubeSat in space, Journal of Applied Remote Sensing, 13, 1, https://doi.org/10.1117/1.jrs.13.032504, https://doi.org/10.1117/1.jrs.13.032504, 2019.

Pickett, H., Poynter, R., Cohen, E., Delitsky, M., Pearson, J., and Müller, H.: SUBMILLIMETER, MILLIMETER, AND MICROWAVE SPECTRAL LINE CATALOG, Journal of Quantitative Spectroscopy and Radiative Transfer, 60, 883–890, https://doi.org/10.1016/s0022-4073(98)00091-0, 1998.

Pougatchev, N., August, T., Calbet, X., Hultberg, T., Oduleye, O., Schlüssel, P., Stiller, B., Germain, K. S., and Bingham, G.: IASI temperature and water vapor retrievals – error assessment and validation, Atmospheric Chemistry and Physics, 9, 6453–6458, https://doi.org/10.5194/acp-9-6453-2009, 2009.

Read, W. G., Shippony, Z., and Snyder, W. V.: EOS MLS Forward Model Algorithm Theoretical Basis Document, Jet Propulsion Lab., JPL D-18130CL#04-2238, Pasadena, CA, USA, 2004, 2004.

Roy, R., Lebsock, M., Millán, L., and Cooper, K. B.: Validation of a G-band differential absorption cloud radar for humidity remote sensing, Journal of Atmospheric and Oceanic Technology, Submitted, 2019.

Roy, R. J., Lebsock, M., Millán, L., Dengler, R., Monje, R. R., Siles, J. V., and Cooper, K. B.: Boundary-layer water vapor profiling using differential absorption radar, Atmospheric Measurement Techniques, 11, 6511–6523, https://doi.org/10.5194/amt-11-6511-2018, https://doi.org/10.5194/amt-11-6511-2018, 2018.

Sassen, K. and Wang, Z.: Classifying clouds around the globe with the CloudSat radar: 1-year of results, Geophysical Research Letters, 35, https://doi.org/10.1029/2007gl032591, https://doi.org/10.1029/2007gl032591, 2008.

Schluessel, P. and Emery, W. J.: Atmospheric water vapour over oceans from SSM/I measurements, International Journal of Remote Sensing, 11, 753–766, https://doi.org/10.1080/01431169008955055, 1990.

Schotland, R. M.: Some observations of the vertical profile of water vapor by means of a ground based optical radar, Proceedings of the Fourth Symposium on Remote Sensing of the Environment, Environmental Research Institute of Michigan, Ann Arbor, MI, USA, pp. 273–283, 1966.

Sekhon, R. S. and Sirvastava, R. C.: Snow size spectra and radar reflectivity,, J. Atmos. Sci., 37, 299–370, https://doi.org/10.1175/1520-0469(1970)027<0299:SSSARR>2.0.CO;2, 1970.

Stephens, G. L., Vane, D. G., Boain, R. J., Mace, G. G., Sassen, K., Wang, Z., Illingworth, A. J., O'Connor, E. J., Rossow, W. B., Durden, S. L., Miller, S. D., Austin, R. T., Benedetti, A., Mitrescu, C., and Team, T. C. S.: THE CLOUDSAT MISSION AND THE A-TRAIN: A New Dimension of Space-Based Observations of Clouds and Precipitation, Bulletin of the American Meteorological Society, 83, 1771–1790, https://doi.org/10.1175/bams-83-12-1771, 2002.

Tian, L., Heymsfield, G. M., Li, L., and Srivastava, R. C.: Properties of light stratiform rain derived from 10- and 94-GHz airborne Doppler radars measurements, Journal of Geophysical Research, 112, https://doi.org/10.1029/2006jd008144, 2007.

Townes, C. H. and Geschwind, S.: Limiting Sensitivity of a Microwave Spectrometer, Journal of Applied Physics, 19, 795–796, https://doi.org/10.1063/1.1698206, 1948.

Walsh, E. J.: Pulse-to-pulse correlation in satellite radar altimeters, Radio Science, 17, 786–800, https://doi.org/10.1029/rs017i004p00786, https://doi.org/10.1029/rs017i004p00786, 1982.

Wang, H., Liu, X., Chance, K., Abad, G. G., and Miller, C. C.: Water vapor retrieval from OMI visible spectra, Atmospheric Measurement Techniques, 7, 1901–1913, https://doi.org/10.5194/amt-7-1901-2014, 2014.

Wentz, F. J.: A well-calibrated ocean algorithm for special sensor microwave / imager, Journal of Geophysical Research: Oceans, 102, 8703–8718, https://doi.org/10.1029/96jc01751, 1997.

Wentz, F. J. and Meissner, T.: AMSR ocean algorithm, version 2, Remote Sensing Systems Tech. Rep. 121599A-1, p. 66p, availablefromhttp://eospso.gsfc.nasa.gov/sites/default/files/atbd/atbd-amsr-ocean.pdf.], 2000.

Wulfmeyer, V. and Walther, C.: Future performance of ground-based and airborne water-vapor differential absorption lidar. II. Simulations of the precision of a near-infrared, high-power system, Appl. Opt., 40, 5321–5336, https://doi.org/10.1364/AO.40.005321, 2001.

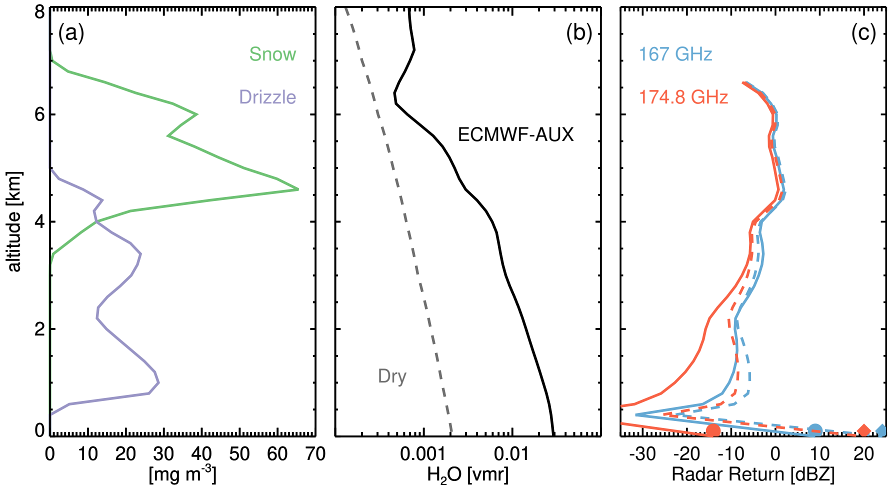

Figure 1. Example of CloudSat driven simulations. (a) Hydrometeor burden. (b) Water vapor burden for two scenarios: the ECMWF-AUX scenario (solid line) and dry case (dash line). (c) CloudSat driven simulations assuming the hydrometeor burden shown in panel A and the two water vapor burden scenarios (solid lines for the ECMWF-AUX scenario and dash lines for the dry case) shown in panel B for the two frequencies used in this study (half circles indicate the magnitude of the surface return in dBZ for the ECMWF-AUX scenario while triangles indicate it for the dry case).

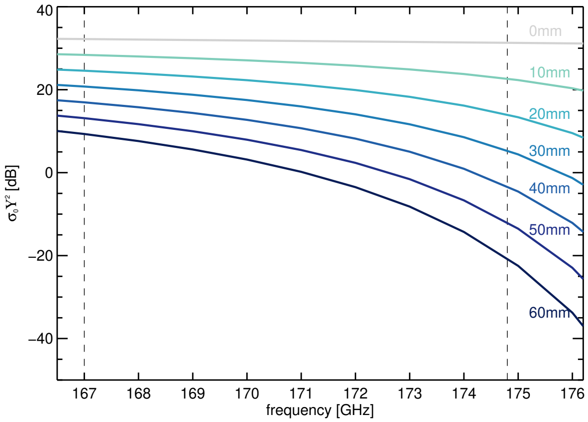

Figure 2. Examples of the spectral variation of the column surface return due to several total column water vapor burdens under clear sky conditions. Dashed vertical lines shows the two frequencies used in this study (167 and 174.8 GHz).

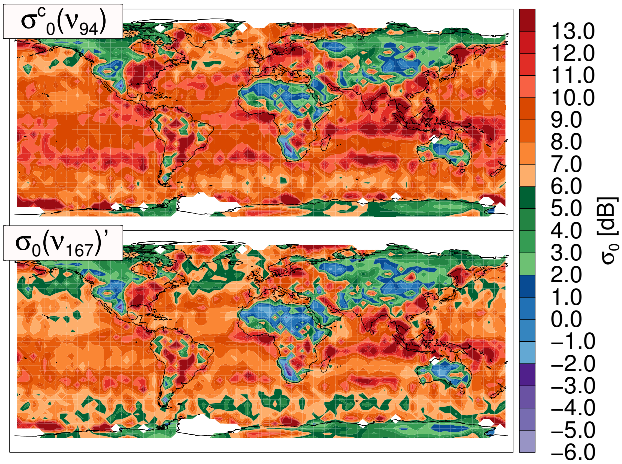

Figure 3. Mean CloudSat surface normalized backscattering cross section for January 1-8, 2007 ($\sigma_0^c(\nu_{94})$), and modified backscattering cross section at 167 GHz ($\sigma_0(\nu_{167})'$). Note that we are displaying the log of the average.

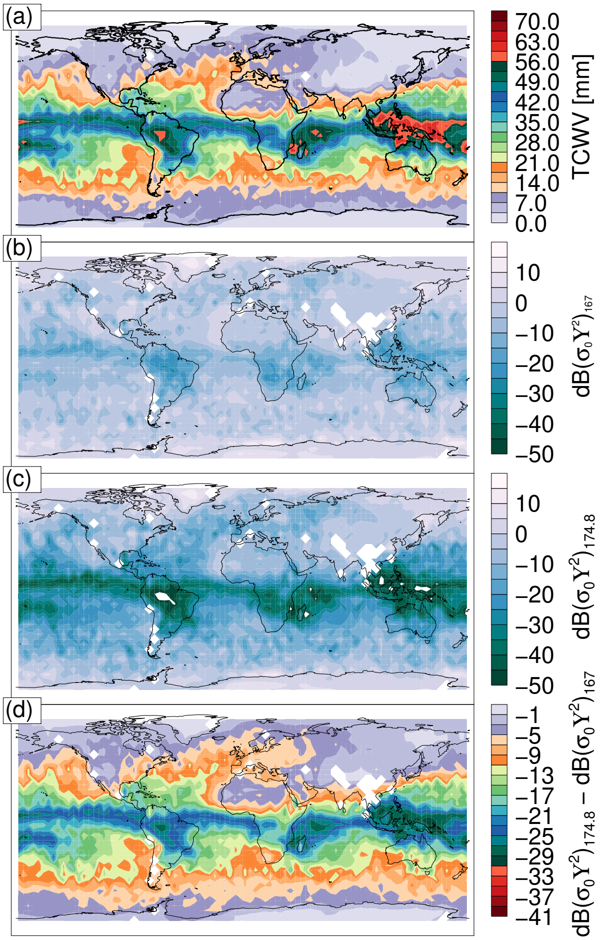

Figure 4. Maps exemplifying the CloudSat driven simulations burdens (January 1-8, 2007). (a) total column water vapor, (b) simulated CloudSat-driven effective surface cross-section at 167 GHz, (c) simulated CloudSat-driven effective surface cross-section at 174.8 GHz, and (d) effective surface cross section difference (174.8–167 GHz). Grid boxes are 4° longitude by 4° latitude.

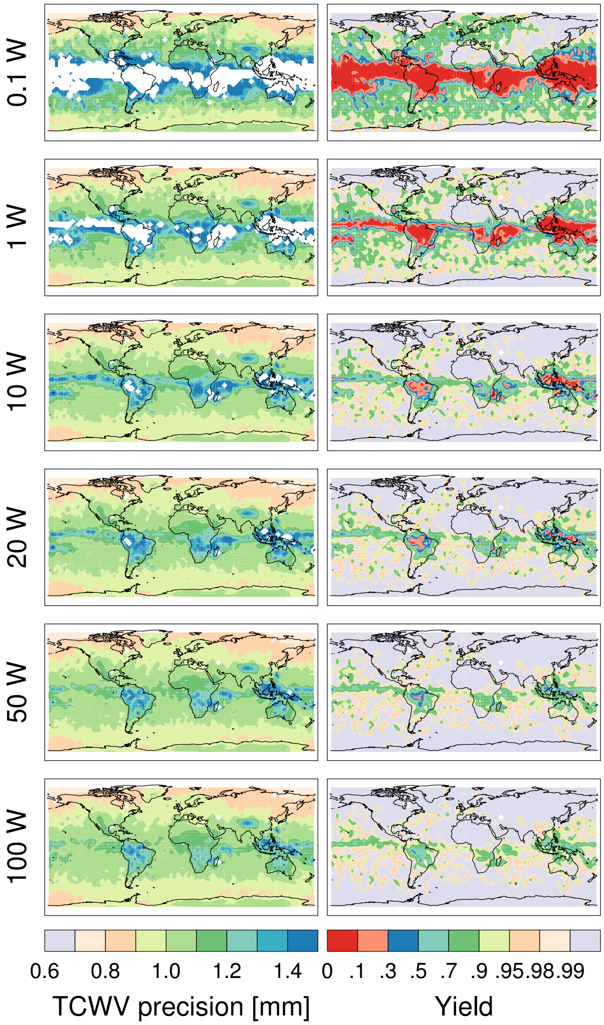

Figure 5. Total column water vapor (TCWV) precision maps as well as fractional yield maps for different transmit powers.

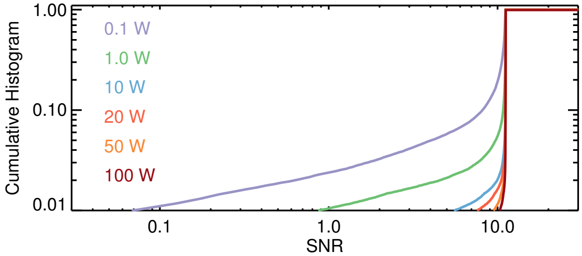

Figure 6. SNR cumulative histogram for the 174.8 GHz radar tone.

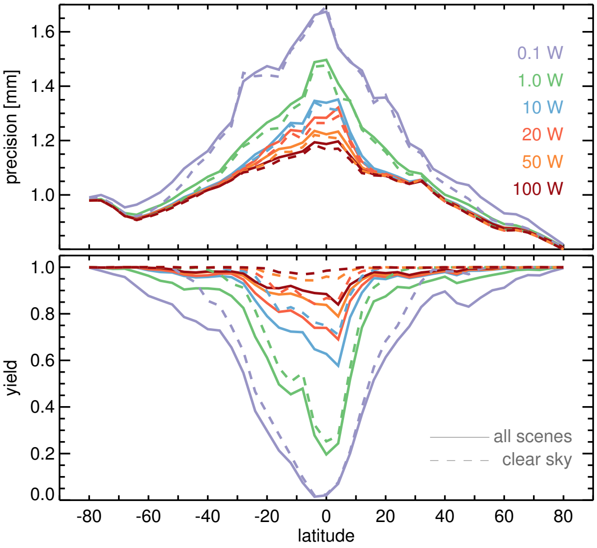

Figure 7. Total column water vapor precision (top) as well as fractional yield (bottom) for different transmit powers versus latitude.

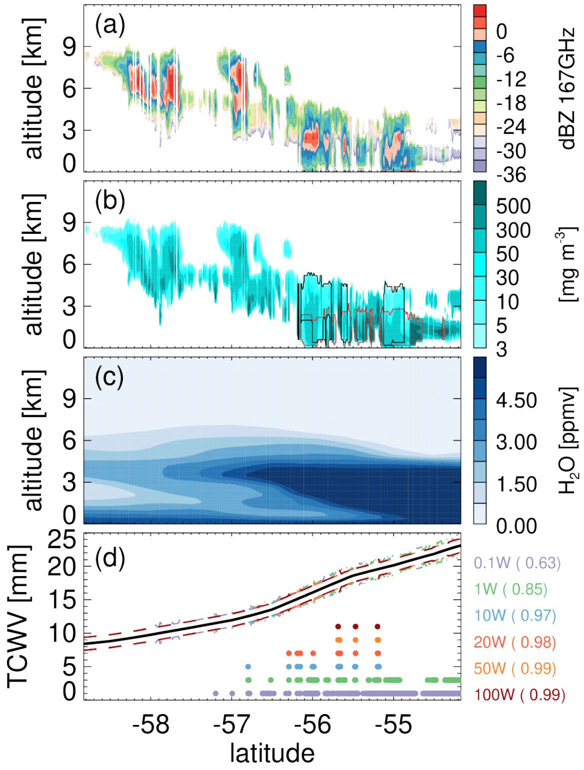

Figure 8. Cross section exemplifying the CloudSat-driven simulations (data from 1 January 2007 over the Southern Ocean). (a) Simulated CloudSat-driven radar reflectivity at 167 GHz. (b) CloudSat retrieved total (IWC+LWC+rain+snow) hydrometeor water content. Black and red lines delimit areas where snow and rain were detected. (c) ECMWF-aux water vapor. (d) Total column water vapor (black solid line) as well as the retrieval precision (dashed lines) for different transmit powers and locations (dots) where at least one of the radar pulses was attenuated beneath the noise floor. Yield values for each simulated transmit powers are given by the numbers in brackets.

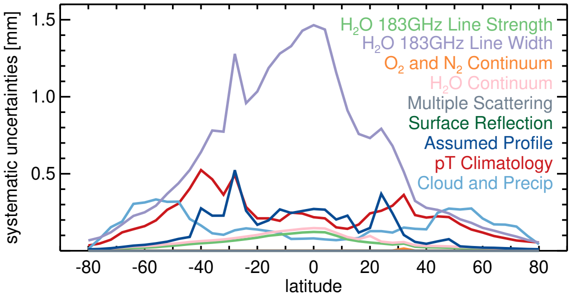

Figure 9. Systematic uncertainties versus latitude

Table 1. Satellite Radar Parameters

Parameter	Symbol	Value	Units
Antenna Diameter	D	1	m
Footprint Diameter		$\sim$850	m
Horizontal Resolution	ΔL	500	m
System Temperature	T_{sys}	1800	K
Platform Altitude	r	405	km
Platform Velocity	V	7669	m/s
Duty cycle	ς	0.25	
Number of pulses	N_P	125	
Chirp time	τ	66	μs
Integration time	T	33	ms
Transmit Powers	P_{T}	0.1, 1, 10, 20, 50, 100	W
Minimum detectable signal[a]	$\sigma_0\ \Upsilon^2$	-18, -28, -38, -41, -45, -48	dB

[a] for each of the transmit powers considered, respectively

Table 2. Radar Instrument Simulator Specifics

Parameter	Detail
Water Dielectric Properties	Liebe et al. (1991)
Ice Dielectric Properties	Hufford (1991)
Ice Water Content (IWC) PSD[a]	McFarquhar and Heymsfield (1997)
Liquid Water Content (LWC) PSD	Using a log normal distribution with a 10 µm mean radius and a 1.3 spread.
Rain PSD	Abel and Boutle (2012)
Snow PSD	Sekhon and Sirvastava (1970)
Gas Absorption	Read et al. (2004)
Radiation Propagation	Hogan and Battaglia (2008); Hogan (2013)
Surface Reflection	Li et al. (2005) assuming climatological surface wind and skin temperature conditions, a Fresnel fraction of 1, and 35 ‰parts per thousand salinity.

[a] particle size distribution.